VELOCITY BUNCHING EXPERIMENT AT SPARC*

D. Filippetto †, D. Alesini, M. Bellaveglia, R. Boni, M. Boscolo, M. Castellano, E. Chiadroni, L. Cultrera, G. Di Pirro, M. Ferrario, L. Ficcadenti, V. Fusco, A. Gallo, G. Gatti, C. Marrelli, M. Migliorati, A. Mostacci, E. Pace,L. Palumbo, B. Spataro, C. Vaccarezza, C. Vicario, LNF-INFN, Frascati,RM, Italy
L. Giannessi, M. Labat, M. Quattromini, C. Ronsivalle, ENEA C.R.Frascati, RM, Italy
A. Bacci, A.R. Rossi, L. Serafini, INFN-Mi, Milano, Italy
M. Serluca, INFN-Roma I, Roma, Italy
A. Cianchi, B. Marchetti, INFN-Roma Tor Vergata, RM, Italy
J. Rosenzweig, UCLA, Los Angeles, CA, USA.

Abstract

The optimization of the beam brightness is one of the main goals of the research and development efforts in rf photo-injectors devoted to short wavelength FELs. The velocity bunching experiment at SPARC has recently demonstrated the possibility of increasing the beam current via rf compression at low energies, while compensating the space charge induced emittance degradation by means of continuous magnetic focusing, increasing the final beam brightness. Stable compression ratios up to a factor 12 and 17 have been observed respectively for the high charge and low charge cases. In this paper measurements of longitudinal beam characteristics, projected and slice transverse emittances in the velocity bunching regime are presented, for different Gun-solenoid field values. Comparisons with simulations are also reported.

INTRODUCTION

The central element of the SPARC machine is the laser driven photo-injector, capable of producing high brightness electron beams. The first element of the machine is a 1.6 cells S-band rf gun (2.856 GHz), followed by 3 S-band traveling wave accelerating structures boosting the electron beam up to 150 MeV. Up to four lines are foreseen downstream the photo-injector, making use of the high brightness beam for different experiments: SASE and seeded FEL experiments [1]; a bypass line with a magnetic chicane for diagnostic and magnetic compression experiments; another two lines for ICS (Inverse Compton Scattering) and plasma acceleration by external injection experiments [2]. All these applications may need high current, low emittance beams. For this reason one of the main goal of SPARC is the experimental demonstration of the beam quality improvement in terms of transverse brightness via the Velocity Bunching technique [3]. In order to keep under control the space charge induced emittance oscillations when the bunch is compressed in the first LINAC section, two long solenoids (TWsol) surround the first two traveling wave sections (Fig. 1).

During the past years the beam compression via velocity bunching scheme have been already experimentally tested in other laboratories [4, 5, 6, 7] but, without a machine layout specifically designed for this kind of process, the emittance compensation has not completely demonstrated, and the final reached beam brightness has not been fully satisfactory.

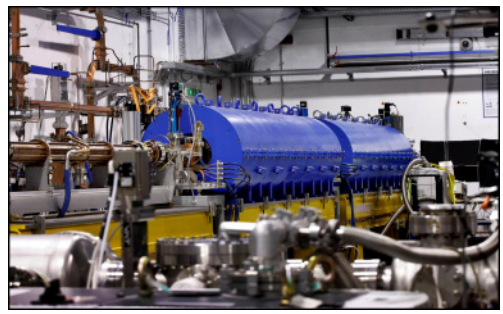

Figure 1: Picture of the SPARC photo-injector showing the 3 accelerating structures with 2 long solenoids.

During the last SPARC run an experimental study of the velocity bunching technique has been performed and the main results are reported in the next sections. Two runs with high (280 pC) and low charge (60 pC) have been carried out, with different compression factors.

THE VELOCITY BUNCHING CONCEPT

The longitudinal phase space rotation in the Velocity Bunching process is based on a correlated velocity chirp in the electron bunch, in such a way that electrons on the tail of the bunch are faster than electrons in the bunch head. This rotation happens inside the longitudinal potential of a traveling rf wave (longitudinal focusing) which accelerates the beam inside a long multi-cell rf structure, applying at the same time an off crest energy chirp to the injected beam [8]. This is possible if the injected beam is slightly slower than the phase velocity of the rf wave so that, when injected at the zero crossing field phase, it will slip back to phases where the field is accelerating, but at the same time it will be chirped and compressed. The key point is that compression and acceleration take place at the same time within the same linac section (rf compressor), usually the first section following the gun, that typically accelerates the beam, under these conditions, from <5 MeV up to 20–25 MeV; the compression takes place in rectilinear trajectory, free from coherent synchrotron radiation emission, which is the primary cause of emittance degradation in magnetic compressors.

* Work partially supported by EUROFEL
† Daniele.Filippetto@lnf.infn.it

The compression factor depends on many parameters: for a fixed compressor injection phase, the initial beam energy, energy spread and bunch length will influence the beam dynamics, change the compression factor and limit the minimum achievable bunch length [8].

THE SPARC DIAGNOSTIC SYSTEM

The SPARC beam diagnostic has been designed to have the possibility to measure all the key parameters needed to fully reconstruct the beam dynamics all along the machine. The rms beam sizes are measured on four screens along the Linac: at the entrance of each rf structure, and at the exit of the linac. After the accelerating sections a 7 meters long beamline (Fig. 2) allows the beam matching to the undulator sections via 2 quadrupole triplets; at the same time it hosts the diagnostic for the incoming beam: the first triplet is used to measure the projected emittance on the emittance screen (Ce:Yag,100 μm thick) by a quadrupole scan [6]; the presence of a dipole magnet allows the measurement of beam energy and energy spread on the spectrometer screen (Ce:Yag,100 μm thick). Moreover an S-band 5 cells standing wave deflector (RFD) can be used in combination with the quad triplet and the dipole magnet to measure the slice longitudinal (bunch length, slice energy spread, longitudinal trace space) and transverse (slice emittance) beam parameters.

At present the deflecting voltage in the RFD is limited to a maximum of 1.5 MV, which leads to a resolution of about 50 fs/pixel at 150 MeV. To calculate the overall measurement resolution one has to take into account also the beam dimensions on the screen when the RFD is switched off [9], which limits the minimum measurable length. For typical SPARC beam sizes of 70 μm the resolution calculated resolution is about 90 fs at 150 MeV, going down to 60 fs for a beam of 100 MeV.

The same holds for spectrometer system resolution: 5 keV/pixel at 150 MeV, and an overall measurement resolution on the relative energy spread of about 0.01%.

VELOCITY BUNCHING EXPERIMENT RESULTS

High Charge Case

In the following we will refer to the slice length (L_s) as the fundamental FEL radiation wavelength (λ_0=500 nm) slippage length calculated for SPARC, i.e. $L_s \approx 250\,\mu$m. In the data analysis procedure the slice of fixed length L_s moves along the bunch in small steps, corresponding to the time resolution of the system.

The laser and machine parameters used for the measurement are reported in Table 1. Also the flat top laser longitudinal shape is showed in Fig. 3. The laser beam dimensions have been chosen considering the needed electron beam charge and the actual rf gun gradient, by scaling the optimum working point for the 1nC case. The 280 pC beam transported to the end of the Linac, reaches an energy of 147.5 MeV, with an rms time duration of 3 ps and a longitudinal shape visible by the blue curve of Fig. 5, leading to a maximum slice current of 30 Amps. In this configuration the three accelerating sections have been tuned in phase for the maximum beam energy at exit.

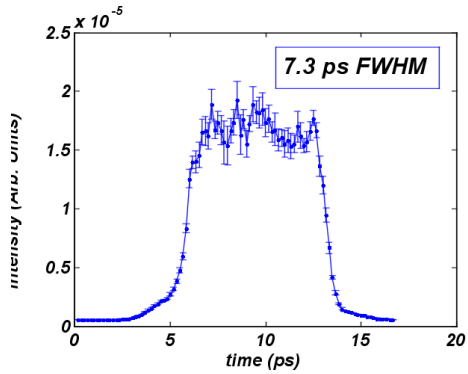

Figure 3: Crosscorrelation measurement of laser beam temporal shape.

By changing the phase of the first accelerating section (*S1*), the bunch length at Linac exit can be varied. Figure 4 shows the rms bunch length for different S1 injection phases. At the maximum compression phase (–95° from the rf crest on Fig. 4) the measured bunch length was 240 fs, leading to a maximum slice current of about 800 Amps. During these measurement the injection phase of the two downstream accelerating sections has been adjusted for the maximum energy. The bunch length has been measured by means of the rf deflector on the emittance screen visible in Fig. 2.

As showed in Table 1, the improvement of beam current takes place to the detriment of beam energy, since the beam in injected on the first section close to the zero crossing phase, correlated energy spread, increasing by one order of magnitude, and transverse emittance, which starts growing because of space charge forces originating from the growing beam current. This emittance growth can be compensated by tuning the long solenoids surrounding the first two accelerating section, keeping under control the beam explosion in the region of lower beam energies.

A moderate compression factor (C) of 3 has been chosen for these measurements. The new beam parameters after the machine tuning are reported in the last column of Table 1 and the achieved beam current is showed by the red curve of Fig. 5.

To compensate for the emittance growth the long solenoids surrounding the first two traveling wave sections have been switched on to current of 45 Amps which corresponds to 450 Gauss of longitudinal magnetic field on-axis. At this point a fine tuning with the gun solenoid has been carried out in order to minimize the projected emittance at the photo-injector end. The resulting emittance scan versus solenoid current is shown in Fig. 6. The solenoid current which gives the minimum overall emittance (the square root of the emittances product) is 157 Amps. An emittance measurement at this working point, switching off TW solenoids, gave emittance values of ϵ_x=6.2 mm·mrad

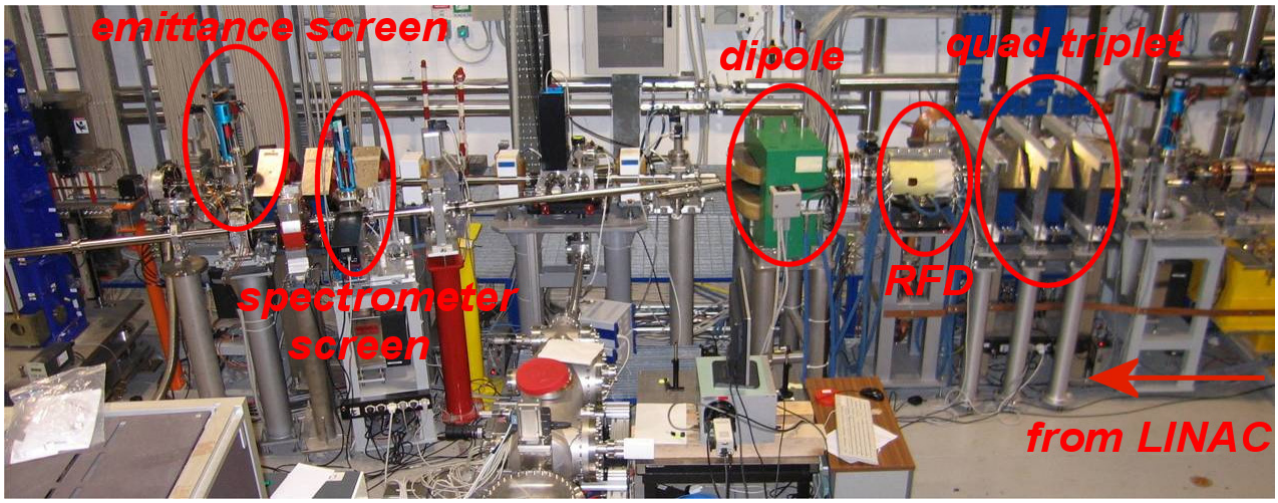

Figure 2: Picture of the beamline used at SPARC for beam matching and diagnostics.

Table 1: Comparison of Beam Parameters for the 280 pC Case, Before (C1) and After (C3) the Compression

	C1	C3
Laser transv. rms X(Y)	358(350) μm	358(350) μm
Laser duration FWHM	7.3 ps	7.3 ps
Gun Peak Field	105 MV/m	105 MV/m
Bunch Charge	280 pC	280 pC
Injection Phase	30 deg	30 deg
Beam Energy	147.5 MeV	101 MeV
Total DE/E rms	0.11 %	1.1 %
Bunch Length rms	3.01 ps	0.97 ps
TW solenoid Field	0 Gauss	450 Gauss
Max slice current	30 Amps	120 Amps

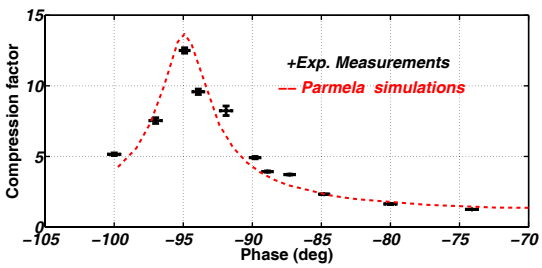

Figure 4: Measured compression factor versus compressor injection phase. The curve reports Parmela simulations of the experiment.

and ϵ_y=4.0 mm·mrad.

As comparison in Fig. 6 is also reported the minimum emittance before compression: it shows a complete emittance compensation in the vertical (Y) plane, but a substantial increase of emittance in the horizontal (X) plane. The reason for this emittance increase is mainly due to the non perfectly aligned solenoid structure, as will become evident

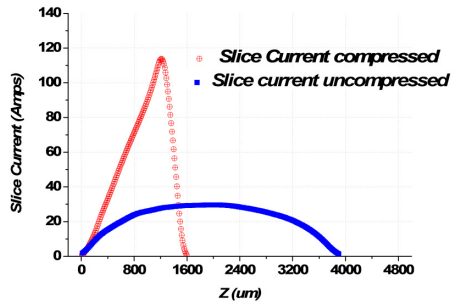

Figure 5: Slice beam current comparison for C=*1* and C=*3*.

in the next chapters.

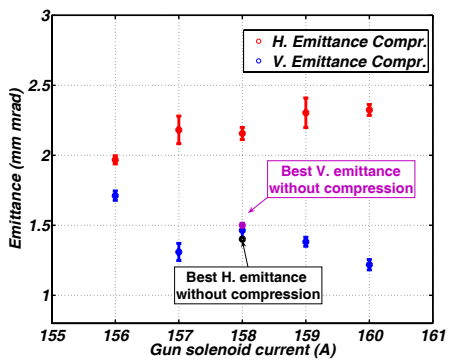

Figure 6: Horizontal and Vertical projected emittance of compressed beam Vs gun solenoid current.

As final tuning measurement, also the horizontal slice emittance for three different gun solenoid currents has been measured, and the results are reported in Figure 7 together with the measured slice current. The growth of the slice emittance values in the bunch tail (left side of the picture) is observed as the gun solenoid field increases; moreover even

if the slice emittance at 157 Amps contains the minimum value, the curve at 160 Amps has its minimum on beam slices with higher currents,leading to higher slice brightness. This is a confirmation that the optimization of projected emittance does not imply the optimization of slice parameters [10].

The maximum compressed beam slice brightness is B_s^{max}=1.1×10^{14} Amps/m^2, compared to the 0.41×10^{14} Amps/m^2 of the uncompressed case.

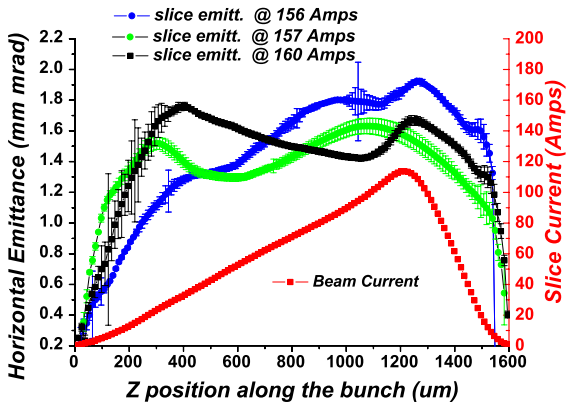

Figure 7: Slice emittance of compressed beam as function of gun solenoid current.

Low charge case

Another run has been dedicated to characterize a low charge beam compressed up to the maximum compression factor possible. The beam parameter that have been changed respect to the previous run are reported in Table 2. The laser time shape has not been changed, so that the beam at the gun exit has a low electron density and is emittance dominated. This is also showed by the fact that the bunch length at Linac exit is much smaller than in the high charge case, due to the reduced space charge contribution to the beam dynamics in the gun region. The low charge beam at the entrance of the compressor has a lower energy spread, and lower longitudinal emittance (54 keV·mm, respect to the 189 keV·mm of the high charge case) and the maximum compression factor achievable in this case is higher than in the high energy experiment.

The laser transverse radius has been reduced to diminish the contribution of the thermal emittance to the total one. A fine tuning of the gun solenoid current has been carried out by measuring the beam emittance at Linac exit for different current values, leading to the final plot of Fig. 8. A minimum emittance of 0.55 µm and 0.57 µm has been found for a solenoid current of 155 Amps.

At this machine working point, also the beam slice emittance has been measured, and all the slices have been found to be below 0.4 µm. The maximum slice current is very low, about 10 Amps (Fig. 9).

Table 2: Comparison of Beam Parameters for the 60 pC Case, Before (C1) and After (C17) the Compression

	C1	C17
Laser transv. rms X(Y)	250(250) µm	250(250) µm
Bunch Charge	60 pC	60 pC
Beam Energy	150 MeV	97.63 MeV
Total DE/E rms	0.11 %	1.1 %
Bunch Length rms	1.935 ps	0.115 ps
Max slice current	10 Amps	217.5 Amps

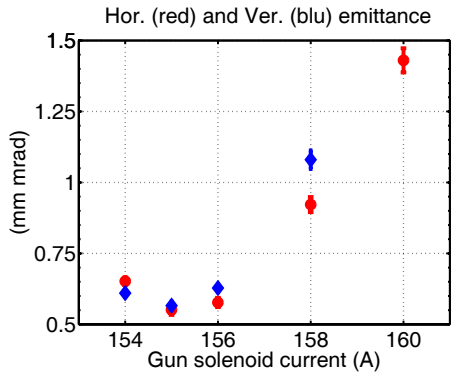

Figure 8: Measured projected emittance versus gun solenoid current (uncompressed beam).

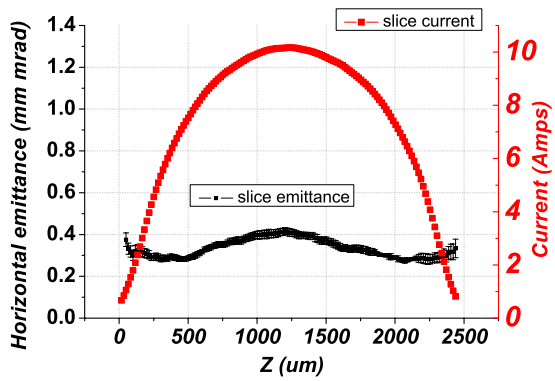

Figure 9: Slice emittance measured for a gun solenoid current of 155 Amps and slice current (uncompressed beam).

The strategy followed to compress the beam is the same described in the previous chapter: the phase of the compressor was varied toward the zero crossing phase, while adjusting the other two sections for the maximum energy gain. In Fig. 10 new C-factor curve is reported, showing three experimental points and the relative simulated curve. The working point corresponding to the maximum compression factor has been chosen as the new working point for beam characterization. The beam current profile is reported in Fig. 11, where the beam is 120 fs rms long, and the maximum current value is 217.5 Amps. One clarifica-

tion is mandatory when comparing the beam current of this beam with the previous ones: in this case the beam length is smaller than the slice width used so far, so that a shorter slice has been used. The slice width in this case coincides with the measurement resolution, i.e 32.5 fs.

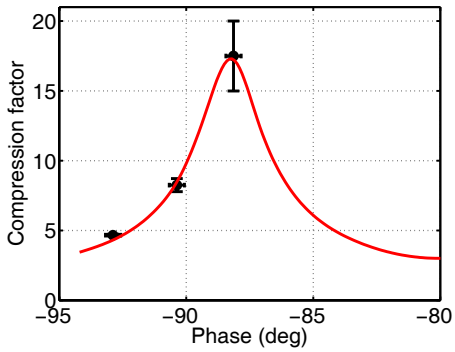

Figure 10: Compression factor versus rf injection phase for the 60 pC case. The red curve shows compression curve simulated by PARMELA.

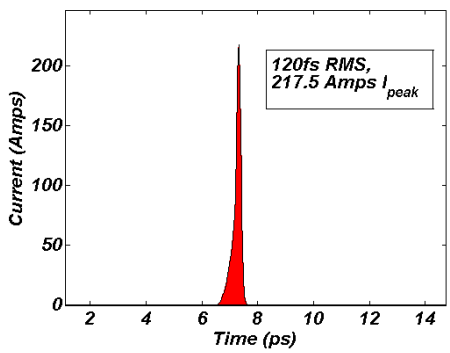

Figure 11: Current profile for the compressed beam.

Figure 12 reports the emittance results obtained with the compressed beam, by scanning the gun solenoid current. Since the beam is very short, system resolution did not allow to measure the slice emittance, and only projected parameters can be measured.

EFFECT OF SOLENOIDS MISALIGNMENT

In the velocity bunching experiment the relative beam energy spread can raise up to few percents inside the compressor section. The particle energy difference is strongly correlated with their relative position inside the bunch itself, as it is the primary cause driving compression. Since the solenoid strength K_s is energy dependent, if the beam propagation axis does not coincides with the solenoid magnetic axis, the beam centroid will move as consequence of the magnetic field. In the case of VB experiment, the strong chirp induced by the rf will cause different slice centroids

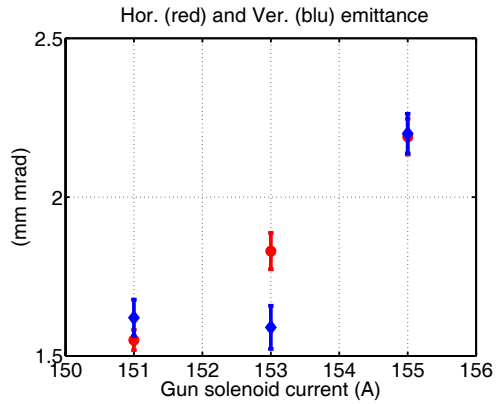

Figure 12: Measured emittances of compressed beam for different gun solenoid currents.

to experience different focusing strength, leading to a beam transverse trace space distortion and emittance increase. As an example, in Figure 13 are reported $X-Z$ and $Y-Z$ simulated planes at Linac exit, for a solenoid horizontal misalignment of 1 mm.

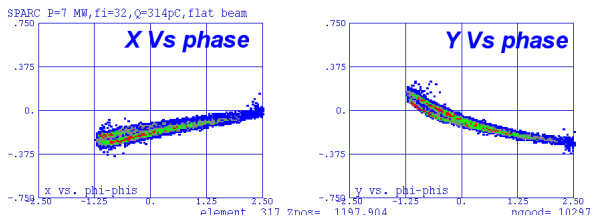

Figure 13: Example of $X-Z$ and $Y-Z$ PARMELA simulated planes for a solenoid misalignment.

An alternative method of calculating the projected emittance is its reconstruction from the slice analysis. The knowledge of the slice emittance and twiss parameters of each slice, together with their relative charge, permits to reconstruct the projected emittance using the formulas written in [12].

Applying these formulas to the slice emittances of Fig. 7, and comparing the resulting values with the horizontal projected emittance values of Fig. 6, leads to the plot shown in Fig. 14. The reconstructed values are sensibly lower than the directly measured ones. This is due to the fact that the above calculation does not includes the ellipse centroid spreads. On the other hand from the quadrupole scan data it is also possible to reconstruct the slice centroid relative positions, both in position ($X_{c,s}$) and in divergence ($X'_{c,s}$).

We took as an example the slice measurement of Fig. 7 relative to a gun solenoid value of 157 Amps. The reconstructed $X-Z$, $X'-Z$ and $X-X'$ planes are showed in Fig. 15. It clearly appears as the slice centroid misalignment in Z results in a distorted projected $X-X'$ trace space, which leads to higher emittances.

The contribution to the projected emittance of the centroid misalignment can be evaluated as already discussed

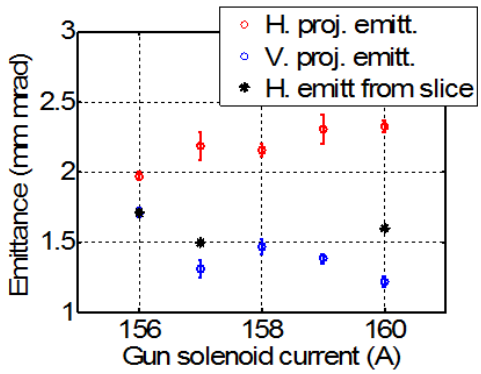

Figure 14: Comparison between measured projected emittances and retrieved from the slice measurements.

in [11], for the case of a uniform flat top beam. The total emittance formula has three contributions: one (ϵ_n^{env}) that depends only from the slice envelopes (calculated respect to their relative centroid); a second term (ϵ_n^{centr}) which represents the emittance of the slice centroids treated as a single particle: it is different from zero only if they do not lie on a straight line; the third term (ϵ_n^{cross}) which correlates the slice centroid positions with their dimension in trace space. Generalizing those formulas for an arbitrary beam, we obtain:

$$\begin{aligned}
\epsilon_n^{env} &= \gamma(\langle\sigma_s^2\rangle\langle\sigma_s'^2\rangle - \langle\sigma_s\sigma_s'\rangle^2)^{1/2};\\
\epsilon_n^{centr} &= \gamma(\langle X_{c,s}^2\rangle\langle X_{c,s}'^2\rangle - \langle X_{c,s}X_{c,s}'\rangle^2)^{1/2};\\
\epsilon_n^{cross} &= \gamma(\langle\sigma_s^2\rangle\langle X_{c,s}'^2\rangle + \langle X_{c,s}^2\rangle\langle\sigma_s'^2\rangle +\\
&\quad -2\langle\sigma_s\sigma_s'\rangle\langle X_{c,s}^2\rangle\langle X_{c,s}'^2\rangle)^{1/2};\\
\epsilon_n^{tot} &= \gamma((\epsilon_n^{env})^2 + (\epsilon_n^{cent})^2 + (\epsilon_n^{cross})^2)^{1/2}; \qquad (1)
\end{aligned}$$

where we omit the $x(y)$ subscript indicating the plane of the measurement; σ_s represents the slice rms envelope. Using these formulas all the three terms in be retrieved for the case of Fig. 15, leading to:

$$\begin{aligned}
\epsilon_{nx}^{env} &= 1.5\,\mu m;\\
\epsilon_{nx}^{centr} &= 0.52\,\mu m;\\
\epsilon_{nx}^{cross} &= 1.72\,\mu m;\\
\epsilon_{nx}^{tot} &= 2.34\,\mu m;
\end{aligned}$$

while the directly measured projected emittance at the point gave $\epsilon_{nx} = 2.3\,\mu m$. The dominant term is the "cross emittance" term, meaning that the emittance is strongly increased by the solenoid misalignment. An on-axis beam would have a projected emittance equal to ϵ_{nx}^{env}.

CONCLUSIONS

In this paper we have experimentally demonstrated the emittance compensation for rf compressed beams. Theory and simulations predict that the emittance explosion caused by the beam density growth could be compensate by the use of long solenoids that focus the electron beam during the compression and the successive acceleration towards high energies, where the space charge force effects are mitigated.

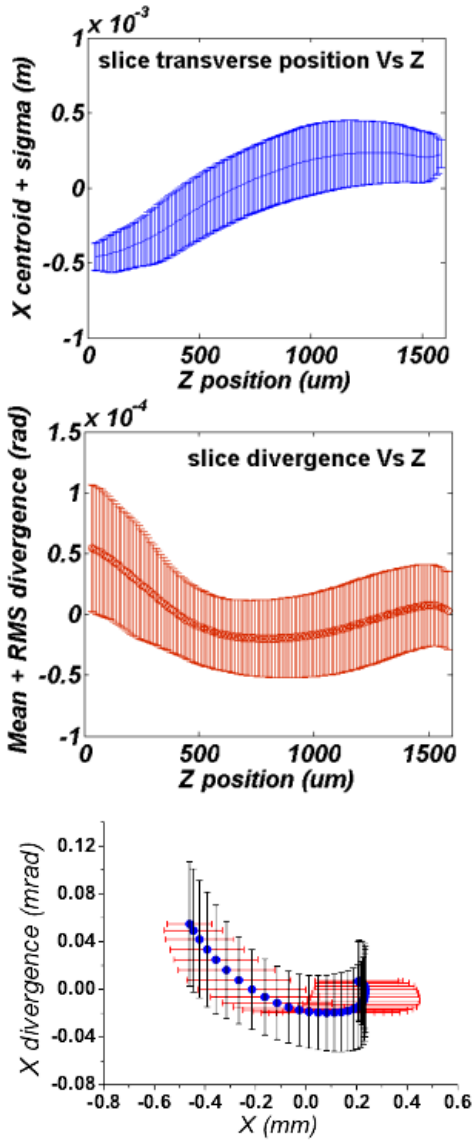

Figure 15: $X-Z$, $X'-Z$ and $X-X'$ planes reconstructed from the slice emittance measurements.

The results reported in this paper shows the experimental validation of that theory: the 280 pC electron beam current has been increased by a factor 4, while maintaining approximately the same emittance value at the end of the photo-injector, i.e. increasing the beam brightness. Measurements and comparison of slice emittances show that also the slice parameters are conserved. This result has been achieved by switching on the long solenoids installed around the accelerating sections, and a fine scan of the gun solenoid to find the right beam matching in the first accelerating section.

Another experiment with a 60 pC beam has been carried out, and the beam has been compressed up to a maximum compression factor of 17. The final beam time duration was 120 fs rms, respect to an initial duration of (1.95 ps rms). The slice emittance of the uncompressed beam was always below 0.4 μm, while the minimum projected emittance (the whole beam is smaller than the slice length) of the compressed beam was about 1.5 μm. Despite this consistent increase of emittance, which is not fully compensated this time, the instantaneous beam current raises up to 217.5 Amps.

A crucial point is the solenoid alignment respect to the rf and beam axis. The high beam energy spread leads to a beam transverse trace space distortion when combined with an off axis magnetic field, with a consequent projected emittance increase. The effect of such misalignment is the introduction of a transverse-longitudinal correlation, that can be calculated from the slice emittance measurements by retrieving the slice centroids in X and X' from the quadrupole scan data. From the formulas 1 the contribution to the projected emittance of this induced correlation can be isolated and calculated.

REFERENCES

[1] L. Giannessi et al., "Seeding experiments at SPARC", Nuclear Instruments and Methods in Physics Research Section A, Volume 593, Issue 1-2, p. 132-136.

[2] A. Bacci et al., "Status of Thomson source at SPARC/PLASMONX", Nuclear Instruments and Methods, A, doi:10.1016/j.nima.2009.05.041.

[3] L. Serafini and M. Ferrario, "Velocity Bunching in Photo-Injectors", AIP Conference Proceedings, 581, 87, (2001).

[4] X.J. Wang et al., "Experimental observation of high-brightness microbunching in a photocathode rf electron gun", Phys. Rev. E 54, R3121 (1996).

[5] S. G. Anderson et al., "Velocity bunching of high-brightness electron beams", Phys. Rev. ST-AB, 8, 014401 (2005).

[6] P. Piot, et al., "Subpicosecond compression by velocity bunching in a photoinjector", Phys. Rev. ST-AB, 6, 033503 (2003).

[7] H. Iijima et al., "Experimental Verification of Velocity Bunching via Shot-by-Shot Measurement at S-Band Photoinjector and Linac", Japanese Journal of Applied Physics Vol. 44, No. 7A, 2005, pp. 52495253.

[8] D.H. Dowell et al., "Slice emittance measurements at the SLACgun test facility", Phys. Rev. ST Accel. Beams 8, 014401 (2005).

[9] D. Alesini et al., "Sliced Beam Parameter Measurements", Proceedings of EPAC 2009.

[10] D.H. Dowell et al., "Slice emittance measurements at the SLACgun test facility", Nuclear Instruments and Methods in Physics Research A 507 (2003) 327330.

[11] M.Ferrario, V.Fusco, M.Migliorati, L. Palumbo,"Emittance degradation due to wake fields in a high brightness photoinjector", Int. Journal of Modern Physics A ,Vol 22, No. 3 (2007) 4214-4234 C.

[12] G. Dattoli, M. Delfranco, P. L. Ottaviani and S. Pagnutti, "Slice Emittance, Projected emittance and properties of the FEL SASE radiation", ENEA internal note,